

Chaos in spin-torque oscillator with feedback circuit

Akira Kamimaki,¹ Tomoyuki Kubota,² Sumito Tsunegi,¹ Kohei Nakajima ², Tomohiro Taniguchi ^{1,*}, Julie Grollier,³ Vincent Cros,³ Kay Yakushiji,¹ Akio Fukushima,¹ Shinji Yuasa,¹ and Hitoshi Kubota¹

¹National Institute of Advanced Industrial Science and Technology (AIST), Research Center for Emerging Computing Technologies, Tsukuba, Ibaraki 305-8568, Japan

²Graduate School of Information Science and Technology, The University of Tokyo, Bunkyo-ku, 113-8656 Tokyo, Japan

³Unité Mixte de Physique, CNRS, Thales, Université Paris-Saclay, 91767, Palaiseau, France



(Received 1 July 2021; accepted 26 November 2021; published 27 December 2021)

Excitation of chaotic magnetization dynamics in nanomagnets is of great interest because it bridges the condensed matter physics and nonlinear science and has a potential to emerging technologies such as neuromorphic computing. However, it has been difficult to observe and identify chaos in spintronics devices because the excitation of chaos requires dynamics in a large-dimensional phase space, according to the Poincaré-Bendixson theorem. An efficient way to overcome this issue is using feedback, which enables the dynamical degrees of freedom to be increased even in a single device. Here, we experimentally demonstrate the excitation of chaos in a vortex spin-torque oscillator by utilizing a feedback circuit. The radio-frequency current emitted by the oscillator flows in the feedback circuit and is converted into an oscillating magnetic field. The oscillating field generates a torque acting on the vortex and modulates its dynamics, resulting in chaotic dynamics which can be tuned by electrical means.

DOI: [10.1103/PhysRevResearch.3.043216](https://doi.org/10.1103/PhysRevResearch.3.043216)

I. INTRODUCTION

Chaos is deterministic but unpredictable nonlinear dynamics with high sensitivity to the initial state. It has been observed in phenomena studied in a wide variety of natural sciences [1–7], including meteorology [4], optics [5], electronics [6], and neuroscience [7], and bridges physics and the other research fields. Moreover, chaos, or highly nonlinear dynamics at the edge of chaos, play fascinating or even sometimes undesirable roles in neuromorphic computing [8–17]. The growing interest in brain-inspired computing using spintronic devices [18–20] has led us to investigate a possibility of exciting and/or controlling chaos in nanomagnets, which may one day lead to the realization of ultrahigh-density solid-state neuromorphic devices. Several proposals have been put forward on how to excite chaos in nanomagnets [21–31], such as by utilizing magnetic multilayers consisting of two free layers [21–23] or applying a periodic current or magnetic field [24–26]. We note that an excitation of chaos in nanomagnets is a challenging task due to the following reason. It has been revealed that the magnetization dynamics is well described by several simplified models, such as macrospin and vortex, with two dynamical degrees of freedom [32]. The validity of these models has been confirmed by experiments. However,

chaos occurs in a phase space larger than two dimensions, according to the Poincaré-Bendixson theorem [2,32]. Therefore, additional factors, such as periodic signal, are necessary to increase the number of degrees of freedom. The previous proposals are inefficient in this sense. For example, the macrospin system with periodic input [24–26] has only three degrees of freedom. In addition, the computational performance of neuromorphic computing, such as in terms of the memory capacity of reservoir computing, is bounded by the dynamical degrees of freedom in the system [33]. Therefore, excitation of chaos in a large dimensional system is highly desired.

An intriguing approach to overcoming these issues is utilizing systems with a feedback signal [34]. The feedback effect inherently exists in natural and artificial systems because of finite speed of signal propagation. However, the number of the experimental investigations on the dynamical systems with time delay had been limited because the time scales in the proposed systems were slow and therefore, the implementation of long time delay was required [35]. For example, it took approximately 20 years to perform the experiment of Mackey-Glass system [36] after its proposal [34]. On the other hand, a fast time scale, on the order of gigahertz, of magnetization dynamics in spintronics devices is advantageous to realize the feedback effect in a relatively simplified circuit. The feedback effect makes the number of degrees of freedom uncountably infinite in principle, and therefore, highly nonlinear (complex) dynamics can be easily excited [35]. In fact, it has been shown that feedback signals in the form of an oscillating current or magnetic field can modulate the amplitude and coherence of the magnetization oscillation in spin-torque oscillators (STOs) [37–41]. An oscillating behavior of a magnetic domain wall driven by direct current was also studied by numerical

*tomohiro-taniguchi@aist.go.jp

Published by the American Physical Society under the terms of the [Creative Commons Attribution 4.0 International](https://creativecommons.org/licenses/by/4.0/) license. Further distribution of this work must maintain attribution to the author(s) and the published article's title, journal citation, and DOI.

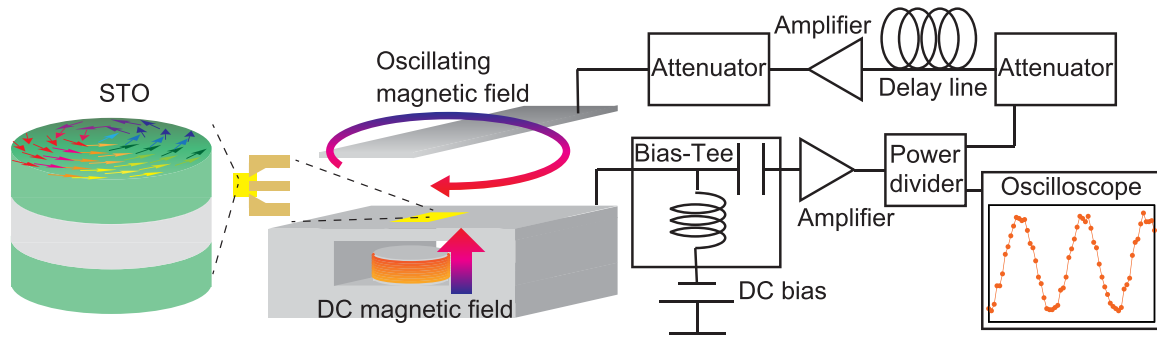


FIG. 1. Schematic illustration of vortex STO with feedback circuit. Direct (bias) voltage injected into the STO excites an oscillation of the vortex through the spin-transfer effect. An external magnetic field is also applied normal to the film plane. The output power is separated from the bias voltage through a bias-tee and is divided into two paths by a power divider. One path is connected to an oscilloscope measuring the vortex dynamics. The other is connected to an attenuator and delay line. The length of the delay line, 50 m, corresponds to the delay time τ of 250 ns. The electric signal passing through the delay line is converted into an oscillating magnetic field, which is applied to the STO as a feedback signal. The feedback signal reflects the past position of the vortex core through the TMR effect.

simulation [42]. These results indicate that spintronics devices are suitable to investigate the complex dynamics caused by the feedback effect experimentally. It has also been found that STOs with a feedback circuit have a large memory capacity in physical reservoir computing [43,44]. However, excitation of chaos in spintronic devices by using a feedback signal has not been experimentally investigated yet, although it was theoretically predicted recently [45–47].

In this study, we report the observation of chaos in a vortex STO with a feedback circuit. Here, the magnetic field generated by the power from the STO is used as a feedback signal. We performed multiple and comprehensive analyses to conclude that the observed nonlinear dynamics are chaotic in nature. We found that chaotic dynamics appear over a wide range of feedback gain above 10–20 dB. These results indicate the tunability of the chaotic state through electrical means, which is a preferable feature for computing applications. Our findings provide an example of chaos in a fine structure and contribute to the deep understanding on the time-delayed system.

The paper is organized as follows. In Sec. II, the materials and device structure of the vortex STO and the feedback circuit are described. In Sec. III, we show three analyses to identify chaos in the STO. Section IV is devoted to the summary and discussion of the present work.

II. MATERIALS AND STRUCTURE OF SPIN-TORQUE OSCILLATOR

Figure 1 is a schematic illustration of the device and circuitry used in this work. The magnetic tunnel junctions (MTJs) used in the study have the following stacking structure: substrate [Si/SiO₂ (500)]/Ta(10)/Cu(40)/Ta(20)/PtMn(5)/CoFe(2.5)/Ru(0.9)/CoFeB(2.5)/MgO(1)/FeB(5)/MgO(1)/Ta(5)/Ru(5) (thickness in nanometers). The nominal diameter is 375 nm. An external magnetic field of 590 mT is applied normal to the film plane. A magnetic vortex is created in the FeB free layer because of its relatively large size and thickness. The magnetization in the CoFe/Ru/CoFeB reference layer is mainly aligned in the film plane but is slightly tilted out of plane due to the external magnetic field

[48]. The perpendicular component of the magnetization in the reference layer provides a perpendicular component to the spin torque acting on the vortex core, which is necessary to induce its self-oscillation [49]. The TMR ratio is about 140%. The device size was designed so that the resistance would be 50 Ω . All experiments were performed at room temperature.

The MTJ is connected to a direct voltage source. Self-oscillation of the gyrotropic motion of the vortex core is excited by the spin transfer effect when the applied voltage becomes larger than a threshold value (150 mV). The applied voltage is subsequently fixed at 225 mV. The input and output powers are separated by the bias-tee shown in Fig. 1. The output power is sent along two paths after passing through the power divider. One path is to an oscilloscope; the other is to a feedback circuit. The gyration of the vortex core is electrically detected using the oscilloscope as an oscillating voltage through the tunnel magnetoresistance (TMR) effect. In addition, part of the output voltage is sent into the feedback circuit, which is constituted by a field line antenna located on top of the STO. The attenuator between the power divider and the delay line and the amplifiers determine the feedback gain. The power of the attenuator is variable, whereas those of the amplifiers are fixed. Accordingly, the feedback gain can be varied from -10 dB to 40 dB. The magnitude of the noise in the amplifiers is at least 10 dB smaller than the power of STO, and therefore, is negligible. Feedback signal flows through the metal line to generate the oscillating magnetic field. Note that the metal line does not match the impedance of the circuit with 50 Ω and reflects the feedback signal. To damp the reflected wave, the other attenuator is connected to the metal line and reduces the standing wave in the circuit. The length of the electrical cable in the feedback circuit is 50 m, corresponding to a delay time of 250 ns. The oscillating magnetic field in turn excites a torque acting on the vortex core that changes its dynamics. Since the magnitude of the delayed feedback signal reflects the position of the vortex core in the past through the TMR effect, the vortex interacts with its past information. As a result, highly nonlinear dynamics are expected [35]. The nonlinearity of the vortex dynamics, as well as the existence of chaos, is analyzed from the power spectra and the dynamic trajectory

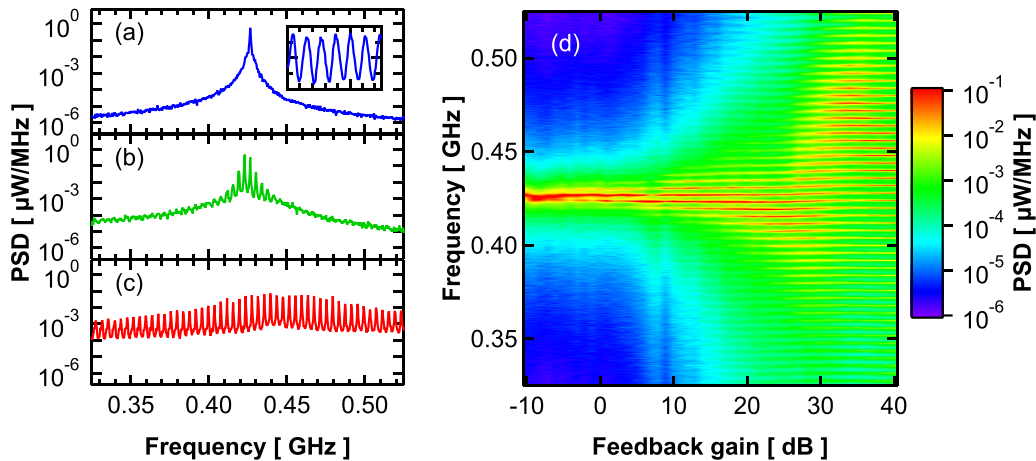


FIG. 2. Power spectra density (PSD) of STO. (a) Time domain signal of the output voltage and its power spectrum density at a low feedback gain of -10 dB. (b),(c) Power spectra density at feedback gains of 15 dB and 40 dB. (d) Power spectra density as a function of feedback gain.

in the embedding space, as well as through a noise-limit estimation.

III. IDENTIFICATION OF CHAOS

In this section, we report three analyses to identify chaos in the STO with the feedback circuit.

A. Spectral analysis

The inset in Fig. 2(a) presents an example of the signal in the time domain of the output voltage at a low feedback gain of -10 dB. The signal is similar to a sinusoidal function with a period of 2.3 ns. A Fourier transformation of such a time trace represents the power spectral density in frequency space and, as shown in Fig. 2(a), it has a single peak at 0.43 GHz. The peak is a typical signature of self-oscillation of the vortex core due to spin-transfer effect with a single well-defined frequency excited in the STO [50]. The spectral shape changes drastically when the feedback gain is increased to 15 dB, as shown in Fig. 2(b). In this case, multiple peaks (in addition to the main peak) appear with an interval of 3.85 MHz, corresponding to the inverse of the delay time (250 ns) of the feedback circuit. The main and the modulation peaks can be easily distinguished, unlike in the case of 40 -dB feedback gain [Fig. 2(c)]. Figure 2(d) summarizes the power spectra densities as a function of feedback gain in which a multipeak structure appears when the feedback gain is larger than 5 dB. We find that the main peak is disappearing for the feedback gain exceeding approximately 20 dB.

There are two possible origins of the multiple peaks. The first one is a periodic oscillation with an amplitude modulation [51,52], while the second possibility is the existence of chaos [45–47]. In the former case, the spectrum has a main peak around which the multiple small peaks appear. On the other hand, in the latter case, the spectral shape becomes broad and several peaks have nearly the same amplitude. It is, however, difficult to distinguish the boundary between the self-oscillation with the amplitude modulation and chaos quantitatively solely from the spectral shape. In addition, we should note that the output signal from the STO does not fully

reflect the actual vortex dynamics; indeed the output signal reflects only the projection of the magnetization direction in the free layer onto the one of the reference layer through the TMR effect. Therefore, the change in the spectral shape might be insufficient information to conclude that chaos appears in the STO. To tackle this issue, we examine two ways to identify the existence of chaos in the STO. The first one is based on the reproduction of the dynamic trajectory in the embedding space, and the second one evaluates the noise limit. In the following, we describe the details of these analyses.

B. Dynamic trajectory in embedding space

An approach to identifying the existence of chaos is to reproduce the dynamic trajectory in an embedding space [53]. We use this method to investigate the relation between the output voltages $v(t)$ and $v(t + \tau_c)$, where the time difference τ_c is determined so that the autocorrelation function of $v(t)$ becomes zero. The map of $v(t)$ and $v(t + \tau_c)$ reflects the dynamic trajectory of the vortex core. For example, if the vortex core shows a circular oscillation in real space, the map of $v(t)$ and $v(t + \tau_c)$ in the embedding space also becomes a circle. As can be seen in this example, the trajectory in the embedding space still reflects the dynamical properties in the original (real) space; see also Appendix A where the result of macrospin simulation based on previous work [46] is given as an example.

Figures 3(a) and 3(b) present the output voltage from the STO and its autocorrelation function for a feedback gain equal to 40 dB. In this case, the time difference τ_c is estimated to be about 0.7 ns. We repeated the estimation of τ_c for several values of the feedback gain.

Figures 3(c)–3(e) illustrate the dynamic trajectories in the embedding space for feedback gains being -10 dB, 15 dB, and 40 dB, respectively. The horizontal and vertical axes are $v(t)$ and $v(t + \tau_c)$, respectively. The trajectory at low gain shown in Fig. 3(c) is circular, indicating an excitation of a periodic self-oscillation of the vortex core in the STO. The small spread of the trajectory is attributed to random motion of the vortex core due to thermal fluctuation. A circular trajectory can be seen until the feedback gain is approximately less than

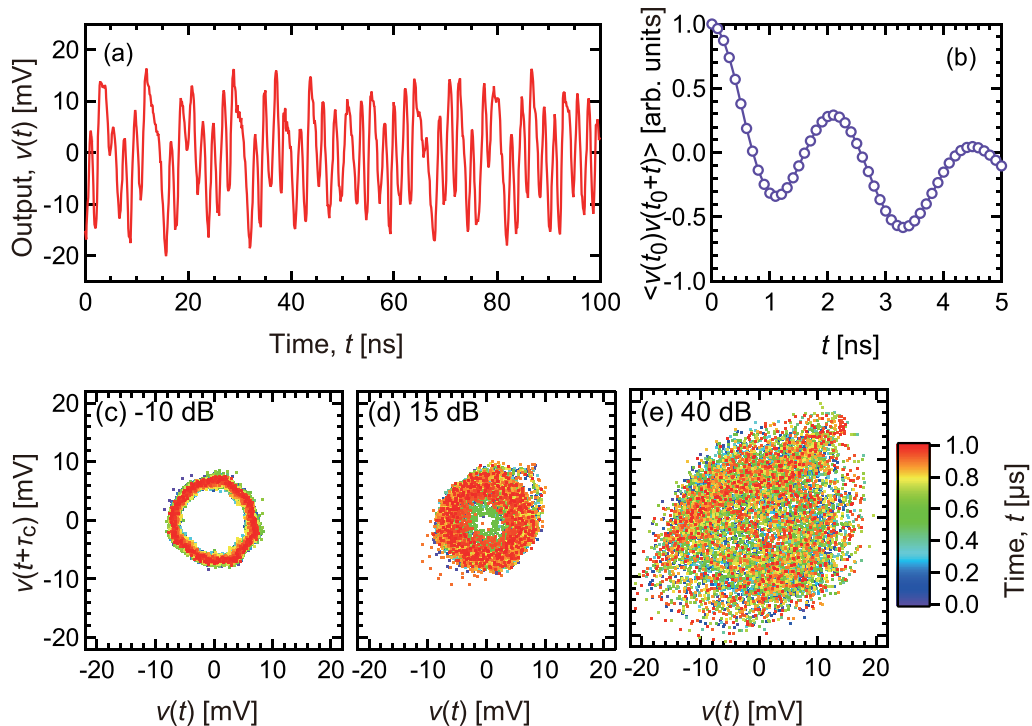


FIG. 3. Dynamical trajectory in embedding space. (a) Time-domain signal of the output voltage and (b) its autocorrelation function at feedback gain of 40 dB. (c)–(e) Dynamic trajectories of the vortex core in the embedding space, where the feedback gains are -10 dB, 15 dB, and 40 dB, respectively.

20 dB. Note that the power spectra densities corresponding to the feedback gain between 5 dB and 20 dB correspond to the case for which the periodic vortex-core dynamics are modulated by the feedback signal; see Sec. III A. However, when the feedback gain is further increased, the trajectory significantly deviates from a circle and covers a large area of the embedding space, as shown in Fig. 3(e).

Two possible origins are considered to explain such a spread of the trajectory. The first one is thermal fluctuation disturbing the vortex-core dynamics randomly, whereas the second one is an appearance of chaos. We should emphasize that thermal fluctuation exists even in a trajectory recorded at the low gain shown in Fig. 3(c). Therefore, the wide spread of the dynamical trajectory found in Figs. 3(d) and 3(e) cannot be attributed to random noise. Accordingly, the results shown in Figs. 3(c)–3(e) imply that chaos appears in the STO with increasing the feedback gain. A highly modulated dynamics may, however, exist in a large feedback-gain region, which makes it difficult to find the boundary between modulated periodic dynamics and chaos. Therefore, we perform time-series analysis in the next section, which can distinguish periodic and chaotic dynamics.

C. Time-series analysis

In this section, we discuss the alternative approach developed in Refs. [54,55] to identifying chaos in our STO. It involves adding white noise to the experimental data and repeating the procedure while increasing the strength of the noise until the nonlinearity of the original data is neutralized by the noise; see also Appendix B. The maximum value of the

standard deviation of the added white noise at which the data with noise still shows nonlinearity is called the noise limit. This method can distinguish chaos from noisy dynamics due to thermal fluctuation and has been used to identify chaos in a different type of STO at 77 K [28]. In addition, the noise limit is zero when the STO falls into a fixed point or shows periodic dynamics. Accordingly, we can identify the existence of chaos from the evaluation of the noise limit by excluding the effect of noise and the possibility of periodic dynamics.

Figure 4 shows the dependence of the noise limit on the feedback gain. The error bars represent the difference of the noise limit with respect to ten different sets of 5000 points of data extracted from the original time series (see Appendix B). The averaged noise limit is less than 10% for feedback gain smaller than 10 dB, indicating that the dynamical state is periodic or weakly chaotic [28,55]; see also Appendix B. On the other hand, the noise limit becomes larger than 10% when the feedback gain is further increased, being a signature of the onset of a strongly chaotic regime [28,55]. This threshold value is slightly different from the one estimated from the spectrum shape and the dynamical trajectory in the embedding space, which might be due to the uncertainty in judging chaos from the spectrum and trajectory, which are subject to gradual changes in their shapes, as well as the data dependence in the estimation of the noise limit (see the error bars in Fig. 4 and Appendix B). The result, however, qualitatively agrees with the other methods and guarantees the existence of chaos.

Note also that noise limit shows nonmonotonic behavior with respect to the feedback gain. Whereas it increases with the feedback gain in low-gain region, the value saturates, or might decrease, in high-gain region. We note that the value of

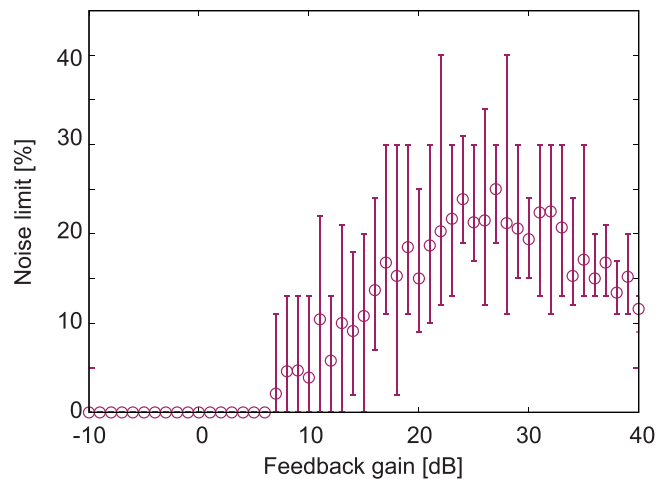


FIG. 4. Noise limit as a function of feedback gain. The bars represent the range of the minimum and maximum values of ten trials in the evaluation. The finite value of the noise limit indicates the existence of chaos.

noise limit often reflects the value of the Lyapunov exponent, although negative and zero Lyapunov exponents cannot be distinguished from the value of noise limit [55]. Assuming that noise limit in the present system also has some correspondence to the Lyapunov exponent, the nonmonotonic behavior of noise limit on the feedback gain in Fig. 4 is similar to the theoretical evaluation of the Lyapunov exponent in macrospin STO with feedback circuit [46]. In Ref. [46], the Lyapunov exponent changes from zero to positive in low-gain region. The Lyapunov exponent, however, begins to decrease at a certain feedback gain and finally becomes zero in high-gain region, where transient chaos appears. The nonmonotonic behavior observed in the present experiment might also indicate an existence of transient chaos. However, further enhancement of the feedback gain is technically difficult, and we had not observed evidence of transient chaos in this work.

IV. DISCUSSION

We have experimentally investigated the existence of chaos in a vortex STO with a feedback circuit. We examined three methods to identify chaos in the STO. First, we evaluated the power spectra density as a function of feedback gain and found an expansion and splitting of the power peak in frequency space. The appearance of a multippeak structure indicates that the dynamical trajectory changes from a simplified circular one to complex orbit due to modulation or chaos. Second, we reproduced the dynamic trajectory in the embedding space, and found a spread of the trajectory covering a wide range of the area dimension in the space. The spread of the trajectory is wider than that found in periodic dynamics, indicating that the spread of the trajectory is also evidence of chaos and it cannot be attributed to thermal fluctuation. Third, we evaluated the noise limit and found that it becomes finite in a large feedback-gain region. These results indicate that chaos appears in the STO when the feedback gain is approximately larger than 10–20 dB.

There are mainly two conditions to efficiently excite chaos by using a feedback signal [35,45–47]. One is to use a large feedback gain, and the other is to make the delay time long. The former strengthens the interaction between the magnetization and its past information, whereas the latter helps to increase the dynamical degrees of freedom. We should emphasize that both requirements are satisfied in the present experiment. For example, the delay time, 250 ns, is two orders of magnitude longer than the oscillation period of the STO that is 2.3 ns. This is the main reason that we can observe chaos by utilizing the feedback effect. In addition, the use of a vortex STO might be beneficial to observing chaos because the vortex structure is relatively robust against disturbances arising from thermal fluctuation. For example, it has been shown that the spectrum linewidth of a vortex STO is one or two orders of magnitude narrower than that of a macrospinlike STO [50]. This fact indicates that the vortex-core dynamics are more deterministic compared with macrospin dynamics even in the presence of random disturbances due to thermal fluctuation. These efficient feedback effects and the robustness against thermal disturbances have made it possible to observe chaos in the STO with a feedback circuit.

The above findings have significance to both fundamental and applied sciences. From the viewpoint of fundamental science, this is an example of chaos in a small world [1–3]. The chaos in nanoscale driven by the feedback effect will be of great interest for further development of nonlinear science on time-delayed dynamical system, where relatively large electric circuits have been used for the experimental implementation [35]. We have excluded the effect of thermal fluctuation to provide solid evidence of chaos because it has been clarified that random motion of the vortex core in STO is non-negligible, although the vortex-type STO has a relatively high thermal stability among spintronics devices, as mentioned above. For practical purposes, the observation of chaos provides a new direction for neuromorphic computing using spintronics technology. Remember that the control of the feedback gain is the trigger of chaos in this study. The tunability between chaotic and nonchaotic states by electronic means would have wide practical applicability. For example, the computational performance in physical reservoir computing could be enhanced by tuning the dynamical state of STO to the edge of chaos [13]. Optimization problems can be solved by using chaotic systems [14]. The present device is thus an important development toward neuromorphic and information sciences.

ACKNOWLEDGMENTS

S.T. and T.T. are grateful to Kenji Watanabe for valuable discussions on time-series analysis. T.T. is also grateful to Shingo Tamaru for valuable discussions on feedback effect in electrical circuits. The results were partially obtained from a project [Innovative AI Chips and Next-Generation Computing Technology Development/(2) Development of next-generation computing technologies/Exploration of Neuromorphic Dynamics towards Future Symbiotic Society] commissioned by NEDO Grant No. JPNP16007. T.K. and K.N. were partially supported by JSPS KAKENHI Grant No.

JP18H05472 and by JST CREST Grant No. JPMJCR2014, Japan.

APPENDIX A: DYNAMIC TRAJECTORY IN EMBEDDING SPACE BY MACROSPIN SIMULATION

The present work is motivated by our previous work [46], where we developed theoretical and numerical analyses on chaos in spin-torque oscillator (STO) driven by feedback circuit. In this previous work [46], we had performed zero-temperature simulation and evaluated the Lyapunov exponent to distinguish chaos from ordered dynamics. Here, we extend it to finite-temperature simulation and compare the dynamical trajectory in the embedding space.

The Landau-Lifshitz-Gilbert (LLG) equation used in the theoretically analysis is given by [46]

$$\frac{d\mathbf{m}}{dt} = -\gamma\mathbf{m} \times \mathbf{H} - \gamma H_s \mathbf{m} \times (\mathbf{p} \times \mathbf{m}) + \alpha \mathbf{m} \times \frac{d\mathbf{m}}{dt} \quad (\text{A1})$$

where \mathbf{m} and \mathbf{p} are the unit vectors pointing in the magnetization directions of the free and reference layers. Note that the STO used in Ref. [46] consists of a perpendicularly magnetized free layer and an in-plane magnetized reference layer. We assume that \mathbf{p} is parallel to the x axis pointing in the in-plane direction. The gyromagnetic ratio and the Gilbert damping constant are γ and α , respectively. The magnetic field $\mathbf{H} = [H_{\text{appl}} + (H_K - 4\pi M)m_z]\mathbf{e}_z$ consists of an applied field H_{appl} , interfacial magnetic anisotropy field H_K , and demagnetization field $-4\pi M$. The spin-transfer torque strength H_s is given by

$$H_s = \frac{\hbar\eta I[1 + \chi\mathbf{m}(t - \tau) \cdot \mathbf{p}]}{2e(1 + \lambda\mathbf{m} \cdot \mathbf{p})MV}, \quad (\text{A2})$$

where M and V are the saturation magnetization and the volume of the free layer, respectively. The spin-transfer torque strength is characterized by the spin polarization η and spin-transfer torque asymmetry λ . The values of the parameters used in this work are derived from the experiment [56], as well as a theoretical analysis [57] as $M = 1448.3$ emu/c.c., $H_K = 18.616$ kOe, $H_{\text{appl}} = 2.0$ kOe, $V = \pi \times 60^2 \times 2$ nm³, $\eta = 0.537$, $\lambda = 0.288$, $\gamma = 1.764 \times 10^7$ rad/(Oe s), and $\alpha = 0.005$. The current of $I = 1.0$ mA corresponds to the current density of 8.8 MA/cm². In the following, we use $I = 2.5$ mA. The strength of the spin-transfer torque, Eq. (A2), includes the feedback current given by $\chi I \mathbf{m}(t - \tau) \cdot \mathbf{p}$, where χ is the rate of the feedback current with respect to the direct current I , whereas τ is the delay time. Due to tunnel magnetoresistance effect, the feedback current depends on the relative direction of the magnetizations, $\mathbf{m} \cdot \mathbf{p}$. Therefore, the feedback current brings in the past information of the magnetization state and extends the dimension of the phase space, which presents a possibility to excite chaotic magnetization dynamics. Note also that random torque $-\gamma\mathbf{m} \times \mathbf{h}$ is added to the right-hand

side of Eq. (A1) to clarify the role of thermal fluctuation on the dynamic trajectory. The components of the random field \mathbf{h} satisfies the fluctuation-dissipation theorem [58],

$$\langle h_k(t)h_\ell(t') \rangle = \frac{2\alpha k_B T}{\gamma MV} \delta_{k\ell} \delta(t - t'). \quad (\text{A3})$$

There are two differences between the previous and present works. Firstly, the magnetic structures are different. The previous work [46] used a macrospin model because the work was motivated by our past experiment [56] using uniformly magnetized free layer. On the other hand, the present experiment uses the vortex STO because it has a relatively large thermal stability [50]. Secondly, the injection methods of the feedback signal are different. The previous work [46] injected the feedback signal to STO as electric current. In contrast, the present experiment converts the feedback signal to magnetic field to avoid electrostatic breakdown by large feedback current. In this Appendix, we use the macrospin model developed in Ref. [46] because the bifurcation points between ordered and chaotic states is already identified by the analysis of the Lyapunov exponent.

We solve the LLG equation numerically and evaluate the dynamic trajectory in the embedding space by the method described in the main text. We use the x component of \mathbf{m} , m_x , as the output signal because it can be measured experimentally through the magnetoresistance effect. Figures 5(a)–5(d) show the trajectories in the embedding space, where the dimensionless feedback gain χ defined in our previous paper and temperature T are (a) $\chi = 0.02$, $T = 0$ K, (b) $\chi = 0.02$, $T = 300$ K, (c) $\chi = 0.5$, $T = 0$ K, and (d) $\chi = 0.5$, $T = 300$ K, respectively. The delay time is $\tau = 30$ ns. Note that the dynamics with $\chi = 0.02$ is modulated dynamics, whereas that with $\chi = 0.5$ is chaos, as clarified by the evaluation of the Lyapunov exponent in our previous work [46]. We firstly notice that the role of temperature is minor. The dynamical trajectory is not disturbed significantly, which might be due to high thermal stability in the free layer. Secondly, the dynamical trajectory is approximately a circle even in the modulated dynamics because the modulation is usually small. On the other hand, the dynamical trajectory is distributed when the system is in chaos. However, the appearance of the distributed trajectory in the embedding space does not necessarily guarantee an existence of chaos; one might consider a possibility that highly modulated dynamics with distributed trajectory are excited in STO. Therefore, to find the boundary between modulated periodic dynamics and chaos, we developed time-series analysis, as mentioned in the main text.

APPENDIX B: DETAIL OF TIME-SERIES ANALYSIS

The noise limit was evaluated by using the second-order discrete Volterra-Wiener-Korenberg (VWK) series defined as [54]

$$y_{c,n} = a_0 + a_1 y_{n-1} + a_2 y_{n-2} + \cdots + a_\kappa y_{n-\kappa} + a_{\kappa+1} y_{n-1}^2 + a_{\kappa+2} y_{n-1} y_{n-2} + \cdots + a_{M-1} y_{n-\kappa}^2 + b_1 y_{n-1-D} + b_2 y_{n-2-D} + \cdots + b_\kappa y_{n-\kappa-D} + b_{\kappa+1} y_{n-1-D}^2 + b_{\kappa+2} y_{n-1-D} y_{n-2-D} + \cdots + b_{M-1} y_{n-\kappa-D}^2 \quad (\text{B1})$$

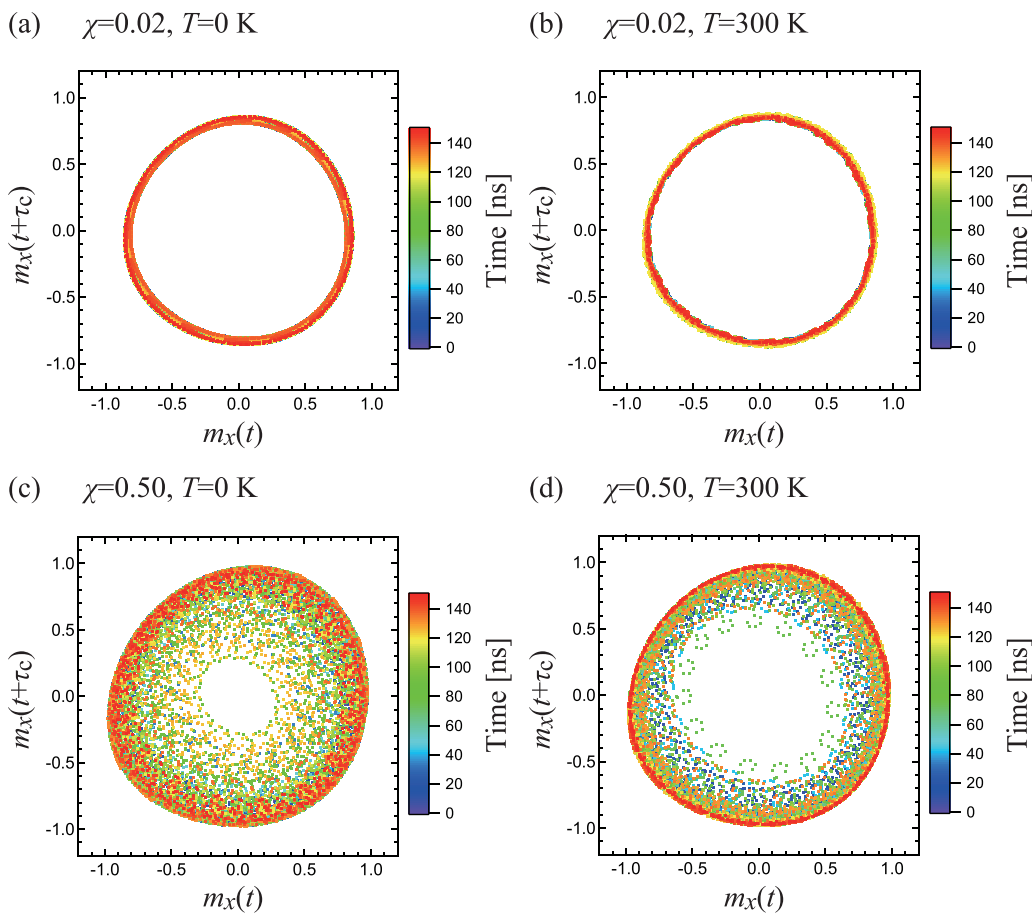


FIG. 5. The dynamical trajectory in the embedding space obtained from macrospin simulation developed in Ref. [46]. The dimensionless feedback-gain parameter χ is 0.02 in (a) and (b) and is 0.5 in (c) and (d). The temperature is zero in (a) and (c), whereas it is 300 K in (b) and (d).

where y_n corresponds to the voltages outputted from the STO at a discrete time n with a time increment of $\Delta t = 0.1$ ns. The expansion coefficients are denoted as a_k and b_k . The memory κ in our analysis was set to 20. The maximum number of terms in the VWK series is $M = (d + \kappa)! / (d! \kappa!)$, where d is the nonlinear dimension and is 2 in Eq. (B1). The VWK series consisting of some of the y_n and their nonlinear combinations is called a truncated VWK series. A linear VWK series including only linear terms of y_n is defined in a similar way. Note that the VWK used in previous works [54] includes terms with the coefficients a_k only. In this work, we add the delay terms with the coefficients b_k with $D = 2500$ because the magnetization dynamics is affected by the feedback effect with the feedback time $\tau = D\Delta t = 250$ ns. The expansion coefficients a_k and b_k are determined through a Gram-Schmidt procedure [54]. The error is defined as

$$\varepsilon^2 = \frac{\sum_{n=1}^N (y_{c,n} - y_n)^2}{\sum_{n=1}^N (y_n - \bar{y})^2}, \tag{B2}$$

where N is the number of data, and \bar{y} is the average of y_n . In our study, we used $N = 5000$ points of data. We investigated the truncated VWK series which minimized the information criterion, $C = \log \varepsilon + (r/N)$, where r is the number of terms in the truncated VWK series.

The noise limit corresponds to the strength of noise necessary to neutralize (or obscure) the nonlinear character in the output data. To evaluate the noise limit, we replaced y_n on the right side of Eq. (B1) with $y_n + \alpha \sigma_y \xi_n$, where σ_y is the standard deviation of y_n , whereas ξ_n is white noise with unit standard deviation. The dimensionless parameter α determines the ratio of the standard deviation of the added noise to σ_y . Using the redefined $y_{c,n}$, the best linear and nonlinear VWK series minimizing the information criterion were investigated again. We repeated the procedure by increasing the value of α until the best nonlinear VWK series provided a significantly better fit to the data y_n than the best linear VWK series by using parametric (F-test) statistics at the 1% significance level. In other words, the procedure was repeated until the errors, ε_L^2 and ε_{NL}^2 , of the linear and nonlinear VWK series satisfied $\varepsilon_L^2 / \varepsilon_{NL}^2 > F$. The standard for the F test was determined from the number of data points N as $F = 1.068$. The noise limit was the minimum value of α at which the relation $\varepsilon_L^2 / \varepsilon_{NL}^2 > F$ was no longer satisfied. To obtain a reliable value of the noise limit, we repeated the above procedure ten times by changing set of 5000 points in the original experimental data. The bars in Fig. 4 represent the range of minimum and maximum values of these ten trials.

We note that noise limit is zero when the dynamical trajectory saturates to a fixed point or limit cycle. Noise limit

often shows good correspondence with the Lyapunov exponent [55], although it cannot distinguish negative and zero Lyapunov exponent. We should, however, be careful that the value of noise limit slightly depends on the choice of data. For example, at the feedback gain of 10 dB, some of ten trials of the evaluation from 5000 points data imply that noise limit is zero; see the bar in Fig. 4. The result indicates that, if we chose a particular 5000 points data the dynamics would

be identified as nonchaotic. To avoid such a case and make our analysis accurate as much as possible, we had used ten sets of different 5000 points data. As can be seen in this example, it is difficult to identify chaos near parameters in which noise limit is finite but close to zero. Therefore, we mentioned that the dynamics is either periodic or weak chaos when noise limit is less than 10%, according to the previous work [28].

-
- [1] S. H. Strogatz, *Nonlinear Dynamics and Chaos: With Applications to Physics, Biology, Chemistry, and Engineering*, 1st ed. (Westview Press, Boulder, 2001).
- [2] K. T. Alligood, T. D. Sauer, and J. A. Yorke, *Chaos. An Introduction to Dynamical Systems* (Springer, New York, 1997).
- [3] E. Ott, *Chaos in Dynamical Systems*, 2nd ed. (Cambridge University Press, Cambridge, 2002).
- [4] E. N. Lorenz, Deterministic nonperiodic flow, *J. Atmos. Sci.* **20**, 130 (1963).
- [5] K. Ikeda and O. Akimoto, Instability Leading to Periodic and Chaotic Self-Pulsations in a Bistable Optical Cavity, *Phys. Rev. Lett.* **48**, 617 (1982).
- [6] P. S. Linsay, Period Doubling and Chaotic Behavior in a Driven Anharmonic Oscillator, *Phys. Rev. Lett.* **47**, 1349 (1981).
- [7] H. Hayashi, S. Ishizuka, M. Ohta, and K. Hirakawa, Chaotic behavior in the onchidium giant neuron under sinusoidal stimulation, *Phys. Lett. A* **88**, 435 (1982).
- [8] C. G. Langton, Computation at the edge of chaos: Phase transitions and emergent computation, *Phys. D: Nonlinear Phenom.* **42**, 12 (1990).
- [9] N. Bertschinger and T. Natschläger, Real-time computation at the edge of chaos in recurrent neural networks, *Neural Comput.* **16**, 1413 (2004).
- [10] D. Sussillo and L. F. Abbott, Generating coherent patterns of activity from chaotic neural networks, *Neuron* **63**, 544 (2009).
- [11] L. Appeltant, M. C. Soriano, G. V. der Sande, J. Danckaert, S. Massar, J. Dambre, B. Schrauwen, C. R. Mirasso, and I. Fischer, Information processing using a single dynamical node as complex system, *Nat. Commun.* **2**, 468 (2011).
- [12] R. Laje and D. V. Buonomano, Robust timing and motor patterns by taming chaos in recurrent neural networks, *Nat. Neurosci.* **16**, 925 (2013).
- [13] J. Nakayama, K. Kanno, and A. Uchida, Laser dynamical reservoir computing with consistency: an approach of a chaos mask signal, *Opt. Express* **24**, 8679 (2016).
- [14] S. Kumar, J. P. Strachan, and R. Williams, Chaotic dynamics in nanoscale NbO₂ Mott memristors for analogue computing, *Nature (London)* **548**, 318 (2017).
- [15] K. Nakajima, Physical reservoir computing - an introductory perspective, *Jpn. J. Appl. Phys.* **59**, 060501 (2020).
- [16] K. Inoue, K. Nakajima, and Y. Kuniyoshi, Designing spontaneous behavioral switching via chaotic itinerancy, *Sci. Adv.* **6**, eabb3989 (2020).
- [17] N. Akashi, T. Yamaguchi, S. Tsunegi, T. Taniguchi, M. Nishida, R. Sakurai, Y. Wakao, and K. Nakajima, Input-driven bifurcations and information processing capacity in spintronics reservoirs, *Phys. Rev. Research* **2**, 043303 (2020).
- [18] J. Grollier, D. Querlioz, and M. D. Stiles, Spintronics nanodevices for bioinspired computing, *Proc. IEEE* **104**, 2024 (2016).
- [19] J. Torrejon, M. Riou, F. A. Araujo, S. Tsunegi, G. Khalsa, D. Querlioz, P. Bortolotti, V. Cros, K. Yakushiji, A. Fukushima, H. Kubota, S. Yuasa, M. D. Stiles, and J. Grollier, Neuromorphic computing with nanoscale spintronic oscillators, *Nature (London)* **547**, 428 (2017).
- [20] J. Grollier, D. Querlioz, K. Y. Camsari, K. Everschor-Sitte, S. Fukami, and M. D. Stiles, Neuromorphic spintronics, *Nat. Electron.* **3**, 360 (2020).
- [21] K. Kudo, R. Sato, and K. Mizushima, Synchronized magnetization oscillations in F/N/F nanopillars, *Jpn. J. Appl. Phys.* **45**, 3869 (2006).
- [22] T. Taniguchi, Synchronized, periodic, and chaotic dynamics in spin torque oscillator with two free layers, *J. Magn. Magn. Mater.* **483**, 281 (2019).
- [23] R. Matsumoto, S. Lequeux, H. Imamura, and J. Grollier, Chaos and Relaxation Oscillations in Spin-Torque Windmill Spiking Oscillators, *Phys. Rev. Appl.* **11**, 044093 (2019).
- [24] Z. Li, Y. C. Li, and S. Zhang, Dynamic magnetization states of a spin valve in the presence of dc and ac currents: Synchronization, modification, and chaos, *Phys. Rev. B* **74**, 054417 (2006).
- [25] Z. Yang, S. Zhang, and Y. C. Li, Chaotic Dynamics of Spin-Valve Oscillators, *Phys. Rev. Lett.* **99**, 134101 (2007).
- [26] T. Yamaguchi, N. Akashi, K. Nakajima, S. Tsunegi, H. Kubota, and T. Taniguchi, Synchronization and chaos in a spin-torque oscillator with a perpendicularly magnetized free layer, *Phys. Rev. B* **100**, 224422 (2019).
- [27] S. Petit-Watelot, J.-V. Kim, A. Ruotolo, R. M. Otxoa, K. Bouzehouane, J. Grollier, A. Vansteenkiste, B. V. de Wiele, V. Cros, and T. Devolder, Commensurability and chaos in magnetic vortex oscillations, *Nat. Phys.* **8**, 682 (2012).
- [28] T. Devolder, D. Rontani, S. Petit-Watelot, K. Bouzehouane, S. Andrieu, J. Letang, M.-W. Yoo, J.-P. Adam, C. Chappert, S. Girod, V. Cros, M. Sciamanna, and J.-V. Kim, Chaos in Magnetic Nanocontact Vortex Oscillators, *Phys. Rev. Lett.* **123**, 147701 (2019).
- [29] A. V. Bondarenko, E. Holmgren, Z. W. Li, B. A. Ivanov, and V. Korenivski, Chaotic dynamics in spin-vortex pairs, *Phys. Rev. B* **99**, 054402 (2019).
- [30] E. A. Montoya, S. Perna, Y.-J. Chen, J. A. Katine, M. d'Aquino, C. Serpico, and I. N. Krivorotov, Magnetization reversal driven by low dimensional chaos in a nanoscale ferromagnet, *Nat. Commun.* **10**, 543 (2019).
- [31] M.-W. Yoo, D. Rontani, J. Letang, S. Petit-Watelot, T. Devolder, M. Sciamanna, K. Bouzehouane, V. Cros, and J.-V. Kim, Pattern generation and symbolic dynamics in a nanocontact vortex oscillator, *Nat. Commun.* **11**, 601 (2020).

- [32] G. Bertotti, I. Mayergoyz, and C. Serpico, *Nonlinear Magnetization Dynamics in Nanosystems* (Elsevier, Oxford, 2009).
- [33] J. Dambre, D. Verstraeten, B. Schrauwen, and S. Massar, Information processing capacity of dynamical systems, *Sci. Rep.* **2**, 514 (2012).
- [34] M. C. Mackey and L. Glass, Oscillation and chaos in physiological control systems, *Science* **197**, 287 (1977).
- [35] D. Biswas and T. Banerjee, *Time-Delayed Chaotic Dynamical Systems: From Theory to Electronic Experiment*, 1st ed. (Springer, Cham, 2018).
- [36] A. Namajunas, K. Pyragas, and A. Tamasevicius, An electronic analog of the Mackey-Glass system, *Phys. Lett. A* **201**, 42 (1995).
- [37] G. Khalsa, M. D. Stiles, and J. Grollier, Critical current and linewidth reduction in spin-torque nano-oscillators by delayed self-injection, *Appl. Phys. Lett.* **106**, 242402 (2015).
- [38] S. Tsunegi, E. Grimaldi, R. Lebrun, H. Kubota, A. S. Jenkins, K. Yakushiji, A. Fukushima, P. Bortolotti, J. Grollier, S. Yuasa, and V. Cros, Self-injection locking of a vortex spin torque oscillator by delayed feedback, *Sci. Rep.* **6**, 26849 (2016).
- [39] D. Kumar, K. Konishi, N. Kumar, S. Miwa, A. Fukushima, K. Yakushiji, S. Yuasa, H. Kubota, C. V. Tomy, A. Prabhakar, Y. Suzuki, and A. Tulapurkar, Coherent microwave generation by spintronic feedback oscillator, *Sci. Rep.* **6**, 30747 (2016).
- [40] H. Singh, K. Konishi, S. Bhuktare, A. Bose, S. Miwa, A. Fukushima, K. Yakushiji, S. Yuasa, H. Kubota, Y. Suzuki, and A. A. Tulapurkar, Integer, Fractional, and Sideband Injection Locking of a Spintronic Feedback Nano-Oscillator to a Microwave Signal, *Phys. Rev. Appl.* **8**, 064011 (2017).
- [41] H. Singh, A. Bose, S. Bhuktare, A. Fukushima, K. Yakushiji, S. Yuasa, H. Kubota, and A. A. Tulapurkar, Self-Injection Locking of a Spin Torque Nano-Oscillator to Magnetic Field Feedback, *Phys. Rev. Appl.* **10**, 024001 (2018).
- [42] J. Williams and J.-V. Kim, A magnetic domain wall Mackey-Glass oscillator, *Appl. Phys. Lett.* **118**, 152404 (2021).
- [43] M. Riou, J. Torrejon, B. Garitane, F. Abreu Araujo, P. Bortolotti, V. Cros, S. Tsunegi, K. Yakushiji, A. Fukushima, H. Kubota, S. Yuasa, D. Querlioz, M. D. Stiles, and J. Grollier, Temporal Pattern Recognition with Delayed-Feedback Spin-Torque Nano-Oscillators, *Phys. Rev. Appl.* **12**, 024049 (2019).
- [44] T. Yamaguchi, N. Akashi, S. Tsunegi, H. Kubota, K. Nakajima, and T. Taniguchi, Periodic structure of memory function in spintronics reservoir with feedback current, *Phys. Rev. Research* **2**, 023389 (2020).
- [45] J. Williams, A. D. Accoily, D. Rontani, M. Sciamanna, and J.-V. Kim, Chaotic dynamics in a macrospin spin-torque nano-oscillator with delayed feedback, *Appl. Phys. Lett.* **114**, 232405 (2019).
- [46] T. Taniguchi, N. Akashi, H. Notsu, M. Kimura, H. Tsukahara, and K. Nakajima, Chaos in nanomagnet via feedback current, *Phys. Rev. B* **100**, 174425 (2019).
- [47] J. Williams and J.-V. Kim, Effects of delayed feedback on the power spectrum of spin-torque nano-oscillators, *J. Phys. D: Appl. Phys.* **53**, 49501 (2020).
- [48] A. Dussaux, B. Georges, J. Grollier, V. Cros, A. V. Khvalkovskiy, A. Fukushima, M. Konoto, H. Kubota, K. Yakushiji, S. Yuasa, K. A. Zvezdin, K. Ando, and A. Fert, Large microwave generation from current-driven magnetic vortex oscillators in magnetic tunnel junctions, *Nat. Commun.* **1**, 8 (2010).
- [49] A. V. Khvalkovskiy, J. Grollier, A. Dussaux, K. A. Zvezdin, and V. Cros, Vortex oscillations induced by spin-polarized current in a magnetic nanopillar: Analytical versus micromagnetic calculations, *Phys. Rev. B* **80**, 140401(R) (2009).
- [50] S. Tsunegi, H. Kubota, K. Yakushiji, M. Konoto, S. Tamaru, A. Fukushima, H. Arai, H. Imamura, E. Grimaldi, R. Lebrun, J. Grollier, V. Cros, and S. Yuasa, High emission power and Q factor in spin torque vortex oscillator consisting of FeB free layer, *Appl. Phys. Express* **7**, 063009 (2014).
- [51] M. R. Pufall, W. H. Rippard, S. Kaka, T. J. Silva, and S. E. Russek, Frequency modulation of spin-transfer oscillators, *Appl. Phys. Lett.* **86**, 082506 (2005).
- [52] P. K. Muduli, Y. Pogoryelov, S. Bonetti, G. Consolo, F. Mancoff, and J. Åkerman, Nonlinear frequency and amplitude modulation of a nanocontact-based spin-torque oscillator, *Phys. Rev. B* **81**, 140408 (2010).
- [53] N. H. Packard, J. P. Crutchfield, J. D. Farmer, and R. S. Shaw, Geometry from a Time Series, *Phys. Rev. Lett.* **45**, 712 (1980).
- [54] M. Barahona and C.-S. Poon, Detection of nonlinear dynamics in short, noisy time series, *Nature (London)* **381**, 215 (1996).
- [55] C.-S. Poon and M. Barahona, Titration of chaos with added noise, *Proc. Natl. Acad. Sci. USA* **98**, 7107 (2001).
- [56] H. Kubota, K. Yakushiji, A. Fukushima, S. Tamaru, M. Konoto, T. Nozaki, S. Ishibashi, T. Saruya, S. Yuasa, T. Taniguchi, H. Arai, and H. Imamura, Spin-torque oscillator based on magnetic tunnel junction with a perpendicularly magnetized free layer and in-plane magnetized polarizer, *Appl. Phys. Express* **6**, 103003 (2013).
- [57] T. Taniguchi, H. Arai, S. Tsunegi, S. Tamaru, H. Kubota, and H. Imamura, Critical field of spin torque oscillator with perpendicularly magnetized free layer, *Appl. Phys. Express* **6**, 123003 (2013).
- [58] W. F. Brown, Jr., Thermal fluctuations of a single-domain particle, *Phys. Rev.* **130**, 1677 (1963).